Simultaneous electron-photon excitation of helium in an Nd:YAG laser field

Kevin M. Dunseath, Mariko Dunseath-Terao

Simultaneous electron-photon excitation of helium in a Nd:YAG laser field

K M Dunseath and M Terao-Dunseath

Institut de Physique de Rennes, CNRS-UMR 6251, Université de Rennes 1, Campus de Beaulieu, 35042 Rennes Cedex, France

Abstract. R-matrix Floquet theory is used to study laser-assisted electron-impact excitation of helium at collision energies close to the He(1s2ℓ) thresholds, in the presence of a Nd:YAG laser field of intensity $10^{10}\,\mathrm{W\,cm^{-2}}$. Strong AC Stark mixing occurs between the 1s2s ^{3}S and 1s2p ^{3}P^o states. The He$^-$(1s2s^2 ^{2}S) resonance gives rise to a series of structures in the integrated cross sections, in particular a dominant peak below the first excitation threshold. Agreement with experiment is very good at low energies, but at higher energies the calculated signal remains small while the experimental results are very negative. The role of multiphoton ionization of the metastable states by the Nd:YAG laser field as a mechanism for signal loss in the experiment is also investigated.

PACS numbers: 34.80.Bm, 34.80.Dp, 34.80.Kw, 34.80.Qb

Submitted to: *J. Phys. B: At. Mol. Phys.*

1. Introduction

While multiphoton ionization has become one of the most studied processes in atomic physics, collisions involving field-dressed continuum states in both the initial and final channels remain difficult to investigate, especially from the experimental point of view. In the context of laser-assisted electron-atom collisions, most existing studies concern free-free scattering in the presence of a low-frequency laser field. Less is known concerning simultaneous electron-photon excitation (SEPE), the process of changing the internal state of an atom through combined collisional and radiative interactions. The most spectacular difference compared to field-free scattering is the appearence of an excitation signal below the associated field-free threshold, with the energy deficit of the incoming electron compensated for by absorption of photons. In atomic units, the final kinetic energy E_f of the scattered electron is related to the initial kinetic energy E_i by $E_\mathrm{f} = E_\mathrm{i} - \Delta\epsilon + N_\gamma\omega$, where $\Delta\epsilon$ is the excitation energy, ω is the angular frequency of the laser and N_γ is the net number of photons exchanged: $N_\gamma > 0$ corresponds to absorption, $N_\gamma < 0$ to emission. The threshold for a particular excitation process is hence replicated at integer multiples of the photon energy ω above and below its (Stark-shifted) field-free position, each new threshold corresponding to excitation accompanied by absorption or emission of a particular number of photons.

As in the case of free-free scattering, most experimental studies of the SEPE process have concentrated on electron-helium scattering in a linearly polarized CO_2 laser field, at energies close to the field-free 1s2ℓ excitation thresholds [1–6]. Rather than performing energy-loss spectroscopy of the low-energy scattered electrons, these experiments used time-of-flight spectroscopy to measure the difference in the production of metastable helium atoms when the laser field is on or off, since this gave a larger signal with a lower signal-to-noise ratio. SEPE of neon and argon in a CO_2 laser field has also been investigated [5]. Theoretical studies have been limited to high collision energies using methods based on the Born approximation [7, 8] or to various low-frequency [9–13] or semi-classical [14] approximations, which attempt to relate the cross section for laser-assisted scattering to those of the corresponding field-free process in a relatively simple way. An exception is our study of SEPE of helium in a CO_2 laser field for collision energies close to the lowest field-free excitation thresholds [15]. We used the *ab initio*, non-perturbative R-matrix Floquet theory to calculate cross sections for production of metastable states, which were found to be in very good agreement with the results of a low-frequency approximation and a semi-classical approach. Agreement with experiment was reasonable.

There are very few results, either experimental or theoretical, for electron-atom scattering in a laser other than CO_2. Indeed, it is only recently that free-free electron-helium scattering in a Nd:YAG laser has been studied experimentally [16]. Some results for the SEPE of helium in a weak Nd:YAG laser (10^5 W cm^{-2}) close to the 1s2s ^{3}S threshold obtained by Mason and Newell are given in the review by Mason [17]. Luan *et al* [18] have also studied the SEPE of helium in a Nd:YAG laser, but at the higher

intensity of $10^{10}\,\mathrm{W\,cm^{-2}}$ and for a geometry in which the incident electron momentum is at 45$^{\mathrm{o}}$ to the laser polarization axis. Unlike other experimental work, Luan *et al* were able to put their measurements of the SEPE signal (defined as the difference of the cross sections for production of metastable helium atoms with and without laser field) on an absolute scale. The main features of their results are a large peak just below the $1s2s\,^3S$ excitation threshold, and a very large negative signal at higher energies. Luan *et al* suggested that the peak is due to the $He^-(1s2s^2\,^2S)$ resonance seen in field-free elastic scattering at a similar energy, but also noted that the results of a semi-classical instantaneous collision approximation [14], which works well for SEPE of helium in a CO_2 laser field [14, 15], also reproduced the general shape of the experimental SEPE signal, albeit with an amplitude about a factor four too small. They speculated that the large negative SEPE signal at higher energies may be due to the loss of metastable states through multiphoton ionization. They estimated an effective multiphoton ionization rate of the order of $7\times10^6\,\mathrm{s^{-1}}$, which is in fact orders of magnitude larger than that predicted by perturbation theory.

In an earlier paper [19], we applied the R-matrix Floquet theory to the study of the SEPE of helium in a Nd:YAG laser field, demonstrating the dominant influence of the $He^-(1s2s^2\,^2S)$ resonance. That work was based on a five-state R-matrix calculation, and only considered the scattering geometry in which the incident electron momentum is parallel to the laser polarization axis. In this paper, we extend our earlier calculations in order to compare directly with the experimental results of Luan *et al*. We also use the R-matrix Floquet theory to investigate multiphoton ionization of the $1s2s\,^3S$ and $1s2p\,^3P^o$ excited states, in particular to see if resonance-enhanced multiphoton ionization (REMPI) via high-lying Rydberg states can yield ionization rates of the same order as that estimated by Luan *et al* and hence provide an explanation for the large negative signal seen in the experimental results.

Atomic units are used unless otherwise stated.

2. Outline of the *R*-matrix Floquet approach

R-matrix Floquet (RMF) theory provides an *ab initio*, non-perturbative framework describing atomic processes in a strong, linearly polarized, spatially homogeneous, monomode laser field. It has been developed over a number of years following the initiative of Burke *et al* [20, 21] and has been successfully applied to the study of multiphoton ionization (MPI), laser-assisted scattering, harmonic generation and laser-induced continuum states. A summary of R-matrix Floquet theory together with particularly illustrative examples of its application can be found for example in the recent books by Burke [22] and by Joachain *et al* [23]. We will hence outline only the features of the theory that are relevant for the discussion of the calculations reported in this paper.

R-matrix Floquet theory combines the R-matrix approach for atomic processes with

a Floquet-Fourier expansion

$$\Psi(\boldsymbol{X}_{N+1},t) = \mathrm{e}^{-\mathrm{i}Et}\sum_{n=-\infty}^{\infty}\mathrm{e}^{-\mathrm{i}n\omega t}\Psi_n(\boldsymbol{X}_{N+1}) \tag{1}$$

to solve the time-dependent Schrödinger equation

$$\mathrm{i}\frac{\partial}{\partial t}\Psi(\boldsymbol{X}_{N+1},t) = \left[H_{N+1} - \frac{\mathrm{i}}{\mathrm{c}}\boldsymbol{A}(t)\cdot\sum_{e=1}^{N+1}\boldsymbol{\nabla}_e + \frac{N+1}{2\mathrm{c}^2}\boldsymbol{A}^2(t)\right]\Psi(\boldsymbol{X}_{N+1},t) \tag{2}$$

of an $(N+1)$-electron system in a linearly polarized electric field $\hat{\boldsymbol{z}}\mathcal{E}_0\cos\omega t$ corresponding to the vector potential $\boldsymbol{A}(t) = \hat{\boldsymbol{z}}A_0\sin\omega t$. The set of space- and spin-coordinates $\boldsymbol{x}_e = \{\boldsymbol{r}_e,\boldsymbol{\sigma}_e\}$ of all the electrons is denoted by $\boldsymbol{X}_{N+1} = \{\boldsymbol{x}_1,\boldsymbol{x}_2,\ldots,\boldsymbol{x}_N,\boldsymbol{x}_{N+1}\}$, and H_{N+1} is the field-free Hamiltonian operator for an atomic system with $N+1$ electrons:

$$H_{N+1} = \sum_{e=1}^{N+1}\left[-\frac{1}{2}\boldsymbol{\nabla}_e^2 - \frac{Z}{r_e}\right] + \sum_{e'>e=1}^{N+1}\frac{1}{|\boldsymbol{r}_e-\boldsymbol{r}_{e'}|}.$$

In the R-matrix approach, it is assumed that the N electrons of the target remain confined in the configuration space delimited by $r_e \le a$, where a is the radial extension of the most diffuse target state included in the calculation. A set of field-dressed target states is obtained by diagonalizing equation (2) for N electrons in a basis of field-free target states, after having transformed into the length gauge in which the radiative interaction near the nucleus is weaker than in the original velocity gauge. Each field-dressed target state i is characterized by its orbital magnetic quantum number M_i, parity π_i and, neglecting relativistic corrections, its spin S_i and spin magnetic quantum number M_{S_i}. The orbital angular momentum L_i of the target is no longer well-defined since the laser polarization axis introduces a preferred direction in space, breaking the spherical symmetry of the system. The quasi-eigenvalues E_i^T of the field-dressed target states thus obtained correspond to the threshold energies characterizing the kinetic energies of the scattered or ionized electron: $E - E_i^T = k_i^2/2$.

In the inner region, defined by $r_e \le a$ for all electrons, equation (2) is also transformed into length gauge and diagonalized in a basis of fully antisymmetrized $(N+1)$-electron wave functions composed of target states coupled to continuum orbitals with zero logarithmic derivatives at $r_e = a$. The diagonalization is performed once for each set of good quantum numbers, comprising the total magnetic number $\mathcal{M}_\mathcal{L}$, the total laser-atom parity Π and the total spin $\mathcal{S}$. The R-matrix elements of the inner region solution (*i.e.* the inverse of the logarithmic derivatives in the reaction channels) can be expressed very simply in terms of the quasi-energies of the $(N+1)$-electron eigenvectors and their amplitudes at $r_e = a$.

The R-matrix outer region is defined as the configuration space where the radial coordinate r of the collisional or ionized electron is larger than a, so that exchange with the target electrons can be neglected. Using a Floquet close-coupling expansion of $\Psi(\boldsymbol{X}_{N+1},t)$, equation (2) reduces to an infinite set of coupled ordinary differential equations. While the interaction of the laser field with the bound electrons is still described in the length gauge, its interaction with the collisional electron is expressed

in the velocity gauge in order to avoid numerical divergences, and the R-matrix is transformed accordingly.

Multiphoton ionization and laser-assisted scattering differ only by the asymptotic boundary conditions applied to equation (2). As the radiative interaction terms in the velocity gauge oscillate indefinitively, it is necessary to perform a time-dependent coordinate transformation into the so-called acceleration frame to define uncoupled asymptotic channels. For multiphoton ionization, outgoing Siegert boundary conditions are imposed, which can be satisfied only at certain complex quasi-energies E: the real part of E corresponds to the AC-shifted (*i.e.* field-dressed) energy of the ionizing state while the negative imaginary part corresponds to half its ionization width Γ. The values of E must be found by an iterative search in the complex plane, usually starting from the field-free real values and gradually increasing the laser intensity I. For laser-assisted scattering of an electron by an atom, the boundary condition is the sum of a plane wave and outgoing spherical waves modulated by the scattering amplitude, in the presence of the laser-dressed target. Cross sections can be obtained from the S-matrix elements as in field-free scattering calculations, except that the S-matrices now depend on the total magnetic quantum number $\mathcal{M}_\mathcal{L}$ since the linearly polarized laser field defines a preferred direction in space. Full details are given in [24].

3. SEPE of helium in a Nd:YAG laser field: results and discussion

The aim of this paper is to interpret the SEPE data for helium measured by Luan *et al* [18] near the He(1s2ℓ) excitation thresholds, with an electron beam incident at an angle $\theta_{\rm in}$ of 45$^{\rm o}$ with respect to the polarization axis of the laser field. The experiment was motivated by the possibility of observing departures from the soft-photon approximation [10, 25]. With a photon energy ten times larger than that of a CO_2 laser, the early onset of the SEPE signal with respect to the field-free threshold is also expected to be clearer. There is however a drawback in attempting to observe laser-assisted processes at shorter wavelengths since perturbation theory predicts that the cross sections vary as λ^4 (see [2] and references therein). Luan *et al* endeavoured to determine the SEPE cross section on an absolute scale, while the experiment cumulates the difficulties of manipulating a low-energy electron beam and a laser beam whose intensity should be strong enough for SEPE signal to be significant but not too strong to avoid ionizing the target before scattering can take place. Indeed, in initial experiments without the incident electron beam, Luan *et al* observed above threshold ionization of the helium ground state with up to 10 extra photons. This, together with the absence of electrons ejected with a kinetic energy less than 2 eV, allowed them to deduce a laser intensity of $1.2 \times 10^{12}\,{\rm W\,cm^{-2}}$ at the focus. By shifting the laser focus away from the electron beam, the intensity was reduced to $10^{10}\,{\rm W\,cm^{-2}}$, at which point multiphoton ionization of the ground state helium atoms was no longer observed. To reduce background noise, both laser and electron beams were pulsed. They covered the collisional energy range up to 100 eV, well above the ionization threshold that cannot be

Table 1. Energies and excitation thresholds for the eleven lowest states of helium. The theoretical values are compared with the accurate, non-relativistic energies taken from chapter 11 of [26] and the thresholds recommended by the National Institute of Standards and Technology (NIST) [27].

	Present (au)	Accurate (au)	Present (eV)	NIST (eV)
$1s^2$ 1^1S	−2.89877	−2.90372	0.0	0.0
1s2s 2^3S	−2.17500	−2.17523	19.695	19.820
1s2s 2^1S	−2.14557	−2.14597	20.496	20.616
1s2p 2^3P^o	−2.13246	−2.13316	20.853	20.964
1s2p 2^1P^o	−2.12270	−2.12384	21.118	21.218
1s3s 3^3S	−2.06862	−2.06869	22.590	22.719
1s3s 3^1S	−2.06061	−2.06127	22.808	22.920
1s3p 3^3P^o	−2.05787	−2.05808	22.882	23.007
1s3d 3^3D	−2.05560	−2.05564	22.944	23.074
1s3d 3^1D	−2.05558	−2.05562	22.945	23.074
1s3p 3^1P^o	−2.05452	−2.05515	22.974	23.087

investigated using the R-matrix Floquet method. The theory is however well suited to the lower collision energies where the most interesting features of SEPE are visible. The energy resolution (full width at half maximum) of the incident electrons was estimated to be $\Delta E_{\rm e}^{\rm FWHM} = 0.5\,{\rm eV}$, almost half the Nd:YAG photon energy. Despite this, Luan *et al* observed a clear structure in the SEPE cross section about 0.3 eV below the $1s2s\,^3S$ threshold which can be attributed only to the SEPE process.

As metastable atoms were detected in the experiment without distinguishing their internal state, a theoretical description needs to sum cross sections for excitation into all possible final states, including those populated by cascade. In the energy range below the He($1s3s\,^3S$) threshold considered in this paper, three (field-free) states can be populated: $1s2s\,^3S$, $1s2s\,^1S$ and $1s2p\,^3P^o$ which decays spontaneously to $1s2s\,^3S$ with a lifetime of about 1 nsec. The $1s2p\,^1P^o$ state mainly decays to the ground state, with a branching ratio of only 10^{-3} to $1s2s\,^1S$ so that its contribution to the SEPE signal can be neglected. We use the same target basis as in [15] and [28], which includes 11 helium states up to $1s3\ell$. The wave functions were built using 6 orbitals: 1s, 2s, 2p, 3s, 3p, 3d, and 6 pseudo-orbitals $\bar{4}$s, $\bar{4}$p, $\bar{4}$d, $\bar{4}$f, $\bar{5}$s, $\bar{5}$p. These were determined using the atomic structure package `CIV3` [29], by optimizing not only the energies but also the oscillator strengths. For convenience, we reproduce table 1 of [15] giving the energies of the 11 states included in our calculations compared with the most accurate values available [26]. The excitation thresholds are also compared to the values recommended by the National Institute of Standards and Technology (NIST) [27]. The present excitation thresholds are slightly too low, mainly due to the error in the ground state energy. A further assessment of the quality of the target state wave functions is provided by the dipole oscillator strengths and transition rates, presented in table 2 of [15] for allowed transitions involving the lowest five target states. The agreement is generally good, with the exception of the

$1s2p\,^1P^o \rightarrow 1s2s\,^1S$ transition where the velocity form of the oscillator strength differs by almost 20% from the length form and the value given by NIST.

In the presence of the laser field, the only good quantum numbers are the total atomic spin, the total (atom + photon) parity and the total atomic magnetic number $\mathcal{M}_\mathcal{L}$, which implies that the number of coupled configurations is considerably larger than in the field-free case. Improving the energy of the ground state as well as the energy differences and oscillator strengths between the excited states would substantially increase the computational resources needed for the R-matrix Floquet calculations. Such an effort would be disproportionate in view of the energy resolution and experimental uncertainty affecting the data.

For the scattering calculations, the size of the R-matrix internal region is fixed at $40\,a_0$, while angular momenta of the scattered electron up to $\ell = 9$ are included in the R-matrix basis expansion, with 20 continuum orbitals per angular momentum. The logarithmic derivative matrix is propagated out to $120\,a_0$, where it is matched with an asymptotic expansion to give the reactance matrix $\mathbf{K}$. We retain 10 components in the Floquet expansion (1) (five absorption and four emission components). For scattering geometries in which the electron is not incident parallel to the laser polarization axis, we include all contributions with $|\mathcal{M}_\mathcal{L}| \leq 5$. A final check of the quality of our basis was performed by comparing the field-free electron-helium scattering cross section for production of metastable helium with other R-matrix results as well as with experiment (see [15] for details). The agreement is generally very good, except with experiment above the $1s2p\,^3P^o$ threshold which is less satisfactory.

As already pointed out in [19], the photon energy of the Nd:YAG laser (1.17 eV) is very close to the energy difference between the $1s2s\,^3S$ and $1s2p\,^3P^o$ states (1.144 eV following the NIST reference values, 1.158 eV in our calculation). In the time-independent Floquet picture, this near one-photon degeneracy leads to a strong (64% – 36%) AC Stark mixing of these states with magnetic quantum number $M_i = 0$. To distinguish such strongly mixed states, we will add '$\sim$' above the letter representing the angular momentum of the dominant component, though of course the state itself does not possess a well-defined angular momentum. In table 2, we present the dominant components of the corresponding field-dressed target states, which we denote respectively by $2\,^3\widetilde{S}$ and $2\,^3\widetilde{P}^o$, for $N = 0$ and $N = 1$. In the state label, N is the multiple of photon energy by which the quasi-energy has been shifted with respect to that of the reference, close to the corresponding field-free state. This dressing appears to have been overlooked by Luan *et al* in their discussion for estimating the production of ^3S metastable states as well as the multiphoton ionization rates.

3.1. Electron incident parallel to the laser polarization axis

In figure 1, we present the cross sections for SEPE into the $2\,^3\widetilde{S}$ and $2\,^3\widetilde{P}^o$ states with $M_f = 0$, for a laser intensity of $10^{10}\,W\,cm^{-2}$ and where the incoming electron beam is parallel to the laser polarization axis. The most striking features are the tall

Table 2. Quasi-energies E with respect to the ground state and dominant eigenvector components of the two target states most strongly mixed by the laser field ($M_i = 0$).

E (eV)	Dominant components	Label
19.669 eV	$-0.581\ ^3\mathrm{S} + 0.814\ ^3\mathrm{P}(N=-1)$	$^3\widetilde{\mathrm{P}}^{\mathrm{o}}(N=-1)$
19.708 eV	$0.814\ ^3\mathrm{S} + 0.581\ ^3\mathrm{P}(N=-1)$	$^3\widetilde{\mathrm{S}}(N=0)$
20.839 eV	$-0.581\ ^3\mathrm{S}(N=1) + 0.814\ ^3\mathrm{P}$	$^3\widetilde{\mathrm{P}}^{\mathrm{o}}(N=0)$
20.878 eV	$0.814\ ^3\mathrm{S}(N=1) + 0.581\ ^3\mathrm{P}$	$^3\widetilde{\mathrm{S}}(N=1)$

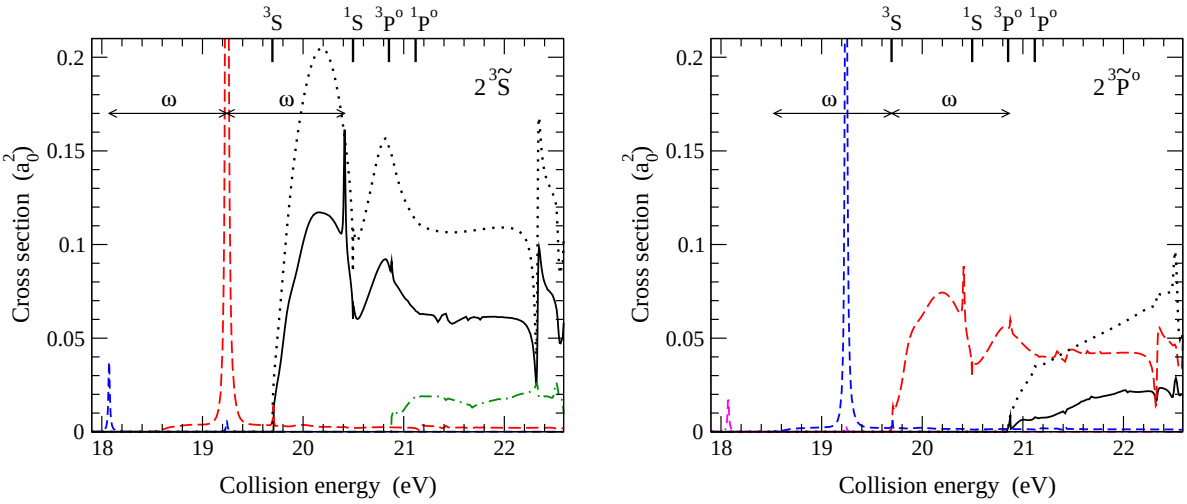

Figure 1. Cross sections for simultaneous electron-photon excitation of helium into the field-dressed $2\,^3\widetilde{\mathrm{S}}$ and $2\,^3\widetilde{\mathrm{P}}^{\mathrm{o}}(M_{\mathrm{f}}=0)$ states, in the presence of a Nd:YAG laser field of intensity $10^{10}\,\mathrm{W\,cm^{-2}}$. The electron is incident parallel to the laser polarization axis. ——, no net exchange of photons; – – –, net absorption of one photon; - - - -, net absorption of two photons; – – · – – –, net absorption of three photons (giving rise to the small peak close to 18.1 eV; right panel only); – · –, net emission of one photon (left panel only). The dotted lines are the corresponding field-free cross sections for excitation into the $2\,^3\mathrm{S}$ and $2\,^3\mathrm{P}^{\mathrm{o}}$ states. The field-free thresholds are indicated along the upper edge of the graphs. In the left panel, the horizontal arrows of length ω indicate the replication of the main $\mathrm{He}^-(1\mathrm{s}2\mathrm{s}^2\,^2\mathrm{S})$ resonance by absorption or emission of one photon. In the right panel, the arrows indicate the similar replication of the $2\,^3\mathrm{S}$ and $2\,^3\mathrm{P}^{\mathrm{o}}$ thresholds.

peaks at a collision energy coinciding with the position of the $\mathrm{He}^-(1\mathrm{s}2\mathrm{s}^2\,^2\mathrm{S})$ resonance observed in field-free elastic scattering below the first excitation threshold. By fitting the field-free elastic phase-shift in the $^2\mathrm{S}$ symmetry, we found the resonance position to be E_{r}=19.244 eV and its width 0.011 eV. The cross section for SEPE into $2\,^3\widetilde{\mathrm{S}}$ with one photon absorption can be easily fitted to the standard Breit-Wigner form since the background is very small and relatively flat as a function of collision energy. The position is unchanged while the width is 0.017 eV, about 50% larger than without laser field. In the presence of the laser field, an electron with an incoming energy of 19.244 eV has a large probability of being captured temporarily in this resonance. The system

may subsequently absorb one photon and decay into the $2\,^3\widetilde{\mathrm{S}}$ excitation channel, or absorb two photons, leading to the production of $2\,^3\widetilde{\mathrm{P}}^{\mathrm{o}}$. The ratio of the heights of the peaks for SEPE with absorption of one photon (left panel of figure 1) and two photons (right panel of figure 1) is about two (see figure 5 below), almost exactly that of the square of the AC Stark mixing coefficients in table 2. Similar peaks appear at collision energies separated by $\pm\omega$ with respect to the resonance at 19.244 eV. In the case of $-\omega$, the electron must first absorb a photon to be temporarily captured in the resonance while in the case of $+\omega$, it must first emit one photon. As the net number of photons exchanged increases by one, the peaks become relatively smaller. The non-resonant part of the cross section for SEPE into $2\,^3\widetilde{\mathrm{S}}$ with one photon absorbed resembles that for no net photon exchange, shifted down in energy by ω and reduced in amplitude by about a factor 30.

At collision energies above the $2\,^3\mathrm{S}$ threshold, the SEPE cross section for $2\,^3\widetilde{\mathrm{S}}$ with no net exchange of photons is similar in form to that for field-free excitation of $2\,^3\mathrm{S}$, but with the amplitude reduced to about 57% of the field-free values. The difference is partially compensated by the cross section for SEPE into $2\,^3\widetilde{\mathrm{P}}^{\mathrm{o}}$ with net absorption of one photon, whose amplitude is about 36% of the field-free cross section for excitation of $2\,^3\mathrm{S}$. This is much more than could be expected from perturbation theory and is a consequence of the AC Stark mixing between the $2\,^3\mathrm{S}$ and $2\,^3\mathrm{P}^{\mathrm{o}}$ states, although their relative contributions do not reflect precisely their respective weights in the wave functions of the $2\,^3\widetilde{\mathrm{S}}$ and $2\,^3\widetilde{\mathrm{P}}^{\mathrm{o}}$ dressed states.

The previous discussion can also be applied to the cross sections for SEPE into $2\,^3\widetilde{\mathrm{S}}$ with net emission of one photon and $2\,^3\widetilde{\mathrm{P}}^{\mathrm{o}}$ with no net exchange of photons. The contribution of the $2\,^3\mathrm{P}^{\mathrm{o}}$ component in the $2\,^3\widetilde{\mathrm{S}}$ is further visible in the cross section into this state with net emission of one photon, with a positive slope above 21.7 eV and resonances above 22.4 eV akin to the field-free $2\,^3\mathrm{P}^{\mathrm{o}}$ excitation cross section.

In figure 2, we present the SEPE cross sections summed over the net number of photons exchanged, from 3 emitted to 4 absorbed. The laser field intensity is 10^{10} $\mathrm{W\,cm^{-2}}$ and the incoming electron beam parallel to the laser polarization axis. The left panel shows results in the triplet final states, while the right pannel shows those for singlet final states. The influence of the laser field is clearly visible below the excitation thresholds where the cross sections without laser field are by definition zero, but the SEPE signature would have been much more difficult to detect had the $\mathrm{He}^-(1\mathrm{s}2\mathrm{s}^2\,{}^2\mathrm{S})$ resonance not been present. In the triplet symmetry, the difference of cross sections with and without the laser field might appear more important than in the singlet symmetry but this is due to the AC Stark mixing of the $2\,^3\widetilde{\mathrm{S}}$ and $2\,^3\widetilde{\mathrm{P}}^{\mathrm{o}}$ states. When the magnetic quantum number of the excited state $2\,^3\mathrm{P}^{\mathrm{o}}$ is ±1, the overall shape of the cross section is similar to that of the field-free cross section since there is no AC Stark mixing with the $2\,^3\mathrm{S}$ state. For a similar reason, the singlet cross sections are also very close to those without laser field. When summed over all possible final metastable states, the difference of the cross sections with and without laser field is expected to be measurable only in the region of the $\mathrm{He}^-(1\mathrm{s}2\mathrm{s}^2\,{}^2\mathrm{S})$ resonance, with eventually smaller side peaks at

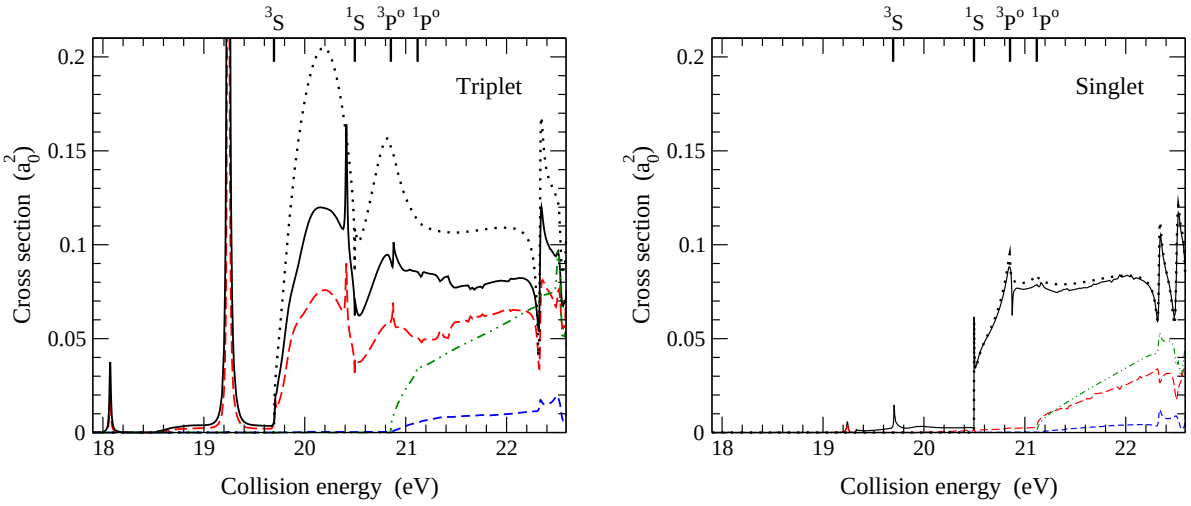

Figure 2. Cross sections for simultaneous electron-photon excitation into the lowest triplet (left) and singlet (right) excited field-dressed states of helium, summed over the number of photons exchanged with the Nd:YAG laser field of intensity $10^{10}\,\mathrm{W\,cm^{-2}}$. The electron is incident parallel to the laser polarization axis. Triplet: ——, excitation into the $2\,^3\widetilde{\mathrm{S}}$ state; – – –, excitation into the $2\,^3\widetilde{\mathrm{P}}^o(M_f = 0)$ state; - - - -, excitation into the $2\,^3\mathrm{P}^o(M_f = \pm 1)$ state; ·····, field-free excitation into the $2\,^3\mathrm{S}$ state; – ·· –, field-free excitation into the $2\,^3\mathrm{P}^o$ state. Singlet: ——, excitation into the $2\,^1\mathrm{S}$ state; – – –, excitation into the $2\,^1\mathrm{P}^o(M_f = 0)$ state; - - - -, excitation into the $2\,^1\mathrm{P}^o(M_f = \pm 1)$ state; ·····, field-free excitation into the $2\,^1\mathrm{S}$ state; – ·· –, field-free excitation into the $2\,^1\mathrm{P}^o$ state.

$E_r \pm \omega$ if the energy resolution and sensitivity of detection are high enough.

3.2. Electron incident at different angles to the laser polarization axis

As the experiment by Luan *et al* has been performed with the electron incoming at an angle $\theta_{in} = 45^o$ with respect to the direction of laser polarisation, we now examine the effect of θ_{in} on the SEPE process. In figure 3, we present the cross sections for SEPE into $2\,^3\widetilde{\mathrm{S}}$ as a function of collision energy up to the $3\,^3\mathrm{S}$ threshold, for a laser intensity of $10^{10}\,\mathrm{W\,cm^{-2}}$ and $\theta_{in} = 0^o, 45^o$ and 90^o, summed over the number of photons exchanged (from 3 emitted to 4 absorbed). The cross section above the $2\,^3\mathrm{S}$ threshold is largest for $\theta_{in} = 90^o$, while above the $2\,^3\mathrm{P}^o$ threshold, it is larger for $\theta_{in} = 0^o$. The differences are usually small except at resonance, in particular at 18.07 eV and 20.41 eV (see insert) where the peak disappears for $\theta_{in} = 90^o$. This is a consequence of conservation of the total parity Π and the total magnetic quantum number $\mathcal{M}_\mathcal{L}$ and can be understood from the expression of the total cross section in terms of the T-matrix elements [24, 30]:

$$\sigma_{if} = \frac{\pi^2}{E_i}\frac{1}{2S_i+1}\sum_{\mathcal{S}}(2\mathcal{S}+1)\sum_{\mathcal{M}\Pi}\sum_{\ell\ell'\ell''} Y^*_{\ell m}(\hat{\boldsymbol{k}}_i)Y_{\ell'' m}(\hat{\boldsymbol{k}}_i)\,T^{\mathcal{M}\Pi\mathcal{S}}_{i\ell m,f\ell' m'}\left(T^{\mathcal{M}\Pi\mathcal{S}}_{i\ell'' m,f\ell' m'}\right)^*. \qquad (3)$$

When the momentum $\hat{\boldsymbol{k}}_i$ of the incoming electron is perpendicular to the direction of polarization of the laser field, the spherical harmonics vanish if the sum of their

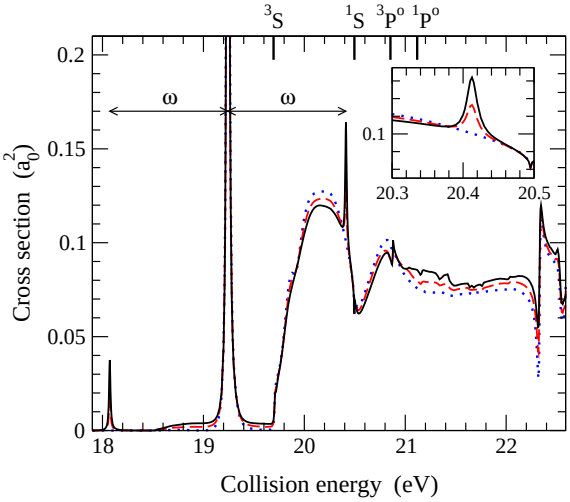

Figure 3. Total cross sections summed over the number of photons exchanged for SEPE into the $2\,^3\widetilde{\mathrm{S}}$ dressed state as a function of collision energy for different angles θ_{in} between the incident electron momentum $\boldsymbol{k}_{\mathrm{i}}$ and the laser polarization axis. ——, $\theta_{\mathrm{in}} = 0^{\mathrm{o}}$; – – –, $\theta_{\mathrm{in}} = 45^{\mathrm{o}}$; ·····, $\theta_{\mathrm{in}} = 90^{\mathrm{o}}$. The resonances at one photon energy below and above the $\mathrm{He}^-(1\mathrm{s}2\mathrm{s}^2\,{}^2\mathrm{S})$ resonance are suppressed for $\theta_{\mathrm{in}} = 90^{\mathrm{o}}$.

indices, $\ell + m$, is odd. The peak at 18.07 eV, one photon energy below the $\mathrm{He}^-(1\mathrm{s}2\mathrm{s}^2\,{}^2\mathrm{S})$ resonance, is due to temporary capture in this resonance by absorption of one photon, followed by absorption of a second photon and excitation of the target into the $2\,^3\widetilde{\mathrm{S}}$ state. Since the parity Π of the resonance is even, the angular momentum ℓ of the collisional electron in the incoming channel must be odd. On the other hand, the magnetic quantum numbers of the target and of the resonance are both zero, so m must be zero too. The sum of the indices of the spherical harmonics in (3) is thus always odd and the resonance at 18.07 eV disappears for $\theta_{\mathrm{in}} = 90^{\mathrm{o}}$. A similar argument explains the disappearance of the resonance at 20.41 eV, which corresponds to the emission of one photon leading to temporary capture, followed by absorption of a second photon and excitation of the target. This selection rule, which depends only on the geometry of the collisional system and the parity of the states involved [30], also applies to the cross sections for SEPE into $2\,^3\widetilde{\mathrm{P}}^{\mathrm{o}}$ presented in figure 4. The peak at 20.41 eV corresponds to temporary capture in the $\mathrm{He}^-(1\mathrm{s}2\mathrm{s}^2\,{}^2\mathrm{S})$ resonance by emission of one photon, followed by absorption of two photons and excitation of the target into the $2\,^3\widetilde{\mathrm{P}}^{\mathrm{o}}(M_{\mathrm{f}} = 0)$ state. This peak (see insert), and its counterpart at 18.07 eV, disappear for $\theta_{\mathrm{in}} = 90^{\mathrm{o}}$. Off resonance, the SEPE cross section is mostly insensitive to the value of θ_{in} up to the $^3\mathrm{P}^{\mathrm{o}}$ threshold, again reflecting the strong AC Stark mixing of the $2\,^3\mathrm{S}$ and $2\,^3\mathrm{P}^{\mathrm{o}}$ states. At higher energies, the cross section into $2\,^3\widetilde{\mathrm{P}}^{\mathrm{o}}(M_{\mathrm{f}} = 0)$ decreases with θ_{in}. For the final state $2\,^3\mathrm{P}^{\mathrm{o}}(M_{\mathrm{f}} = \pm 1)$, the variation of the cross section as a function of θ_{in} is reversed and relatively larger in magnitude.

In figure 5, we present the cross sections for SEPE into $2\,^3\widetilde{\mathrm{S}}$ and $2\,^3\widetilde{\mathrm{P}}^{\mathrm{o}}(M_{\mathrm{f}} = 0)$ in the region of the $\mathrm{He}^-(1\mathrm{s}2\mathrm{s}^2\,{}^2\mathrm{S})$ resonance, for $\theta_{\mathrm{in}} = 0^{\mathrm{o}}, 45^{\mathrm{o}}$ and 90^{o}. The results have been

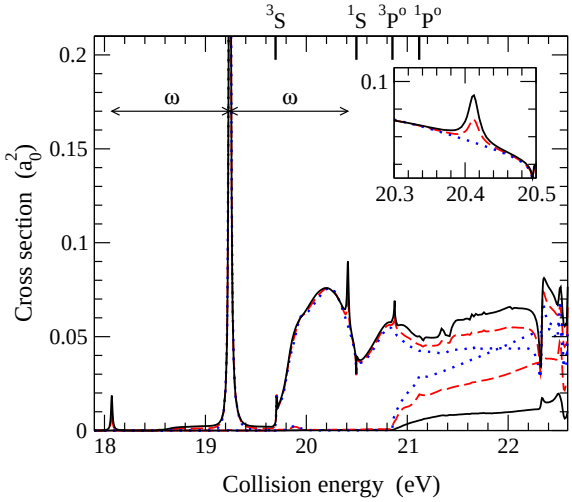

Figure 4. Total cross sections summed over the number of photons exchanged for SEPE into the $2\,^3\widetilde{\mathrm{P}}^{\mathrm{o}}(M_{\mathrm{f}}{=}0)$ (upper curves) and the $2\,^3\mathrm{P}^{\mathrm{o}}(M_{\mathrm{f}} = \pm 1)$ (lower curves starting at the $2\,^3\mathrm{P}^{\mathrm{o}}$ threshold) states as a function of collision energy for different angles θ_{in} between the incident electron momentum $\boldsymbol{k}_{\mathrm{i}}$ and the laser polarization axis. ——, $\theta_{\mathrm{in}} = 0^{\mathrm{o}}$; – – –, $\theta_{\mathrm{in}} = 45^{\mathrm{o}}$; ·····, $\theta_{\mathrm{in}} = 90^{\mathrm{o}}$. The resonances at one photon energy below and above the $\mathrm{He}^-(1\mathrm{s}2\mathrm{s}^2\,{}^2\mathrm{S})$ resonance are suppressed for $\theta_{\mathrm{in}} = 90^{\mathrm{o}}$. Above the $2\,^3\mathrm{P}^{\mathrm{o}}$ threshold, the cross sections are more sensitive to θ_{in} than those for SEPE into the $2\,^3\widetilde{\mathrm{S}}$ dressed state, in particular for $M_{\mathrm{f}} = \pm 1$.

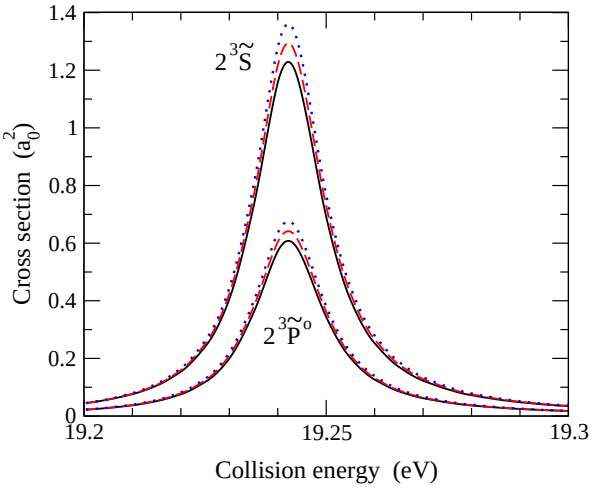

Figure 5. The $\mathrm{He}^-(1\mathrm{s}2\mathrm{s}^2\,{}^2\mathrm{S})$ resonance in the total cross sections (summed over the number of photons exchanged) for SEPE into the $2\,^3\widetilde{\mathrm{S}}$ and $2\,^3\widetilde{\mathrm{P}}^{\mathrm{o}}(M_{\mathrm{f}} = 0)$ dressed states, for different values of the angle θ_{in} between the incident electron momentum $\boldsymbol{k}_{\mathrm{i}}$ and the laser polarization axis. ——, $\theta_{\mathrm{in}} = 0^{\mathrm{o}}$; – – –, $\theta_{\mathrm{in}} = 45^{\mathrm{o}}$; ·····, $\theta_{\mathrm{in}} = 90^{\mathrm{o}}$. In both cases, the maximum increases by approximately 11% as θ_{in} is varied from 0^{o} to 90^{o}, while their ratio remains close to 2.

summed over the number of photons exchanged: from 3 emitted to 4 absorbed, which is sufficient to ensure convergence for a laser intensity of $10^{10}\,\mathrm{W\,cm^{-2}}$. As this resonance

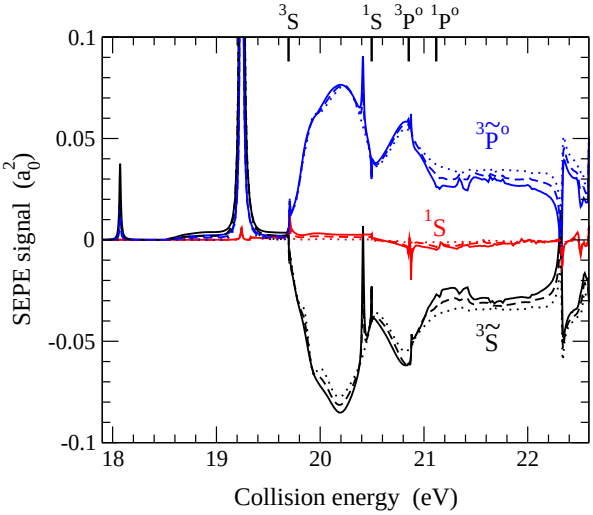

Figure 6. SEPE signals (difference between the laser-assisted and field-free cross sections) for excitation into the $2\,^3\widetilde{\mathrm{S}}$, $2\,^1\mathrm{S}$ and $2\,^3\widetilde{\mathrm{P}}^o(M_f = 0, \pm 1)$ dressed states, for different values of the angle θ_{in} between the incident electron momentum $\boldsymbol{k}_i$ and the laser polarization axis. ——, $\theta_{in} = 0^o$; – – –, $\theta_{in} = 45^o$; · · · · · ·, $\theta_{in} = 90^o$.

is an S state, the cross sections do not vary much as a function of the orientation of the collisional system in the laser field, the difference being at most 11%. At all angles, the ratio of the two peaks is about 2, almost exactly that of the square of the AC Stark mixing coefficients in table 2.

In figure 6, we present the SEPE signals for the final states $2\,^3\widetilde{\mathrm{S}}$, $2\,^3\widetilde{\mathrm{P}}^o(M_f = 0, \pm 1)$ and $2\,^1\mathrm{S}$, *i.e.* the difference of the SEPE cross sections and the corresponding field-free excitation cross sections into $2\,^3\mathrm{S}$, $2\,^3\mathrm{P}^o$ and $2\,^1\mathrm{S}$. Below the $2\,^3\mathrm{S}$ threshold, SEPE mainly occurs through temporary capture in the $\mathrm{He}^-(1s2s^2\,^2\mathrm{S})$ resonance. Above this threshold, the $2\,^3\widetilde{\mathrm{S}}$ signal (mainly with 0 or 1 photon emitted) is negative since its AC Stark mixing with the $2\,^3\mathrm{P}^o$ state leads to a transfer of population into $2\,^3\widetilde{\mathrm{P}}^o$, whose SEPE signal (mainly with 1 or 0 photons absorbed) is large and positive. The sum of the SEPE signals for excitation into $2\,^3\widetilde{\mathrm{S}}$ and $2\,^3\widetilde{\mathrm{P}}^o$ however is very small, except below the $2\,^3\mathrm{S}$ threshold. The SEPE signal for $^1\mathrm{S}$ is very small except at the $2\,^3\mathrm{P}^o$ threshold, characterized by a sharp structure.

3.3. Comparison with experiment

To compare with the SEPE signal measured by Luan *et al*, we sum our values of the SEPE cross sections over the possible final states leading to production of metastable states, *i.e.* the $2\,^3\widetilde{\mathrm{S}}$, $2\,^1\mathrm{S}$ and $2\,^3\widetilde{\mathrm{P}}^o(M_f = 0, \pm 1)$ states, subtract the field-free cross sections for excitation into the $2\,^3\mathrm{S}$, $2\,^1\mathrm{S}$ and $2\,^3\mathrm{P}^o$ states and convolve over the energy spread of the electron beam (assumed to be a Gaussian of FWHM equal to 0.5 eV). In doing so, we assume that all $2\,^1\mathrm{P}^o$ excited states produced during the collision decay rapidly to the ground state and therefore will not contribute to the measured signal.

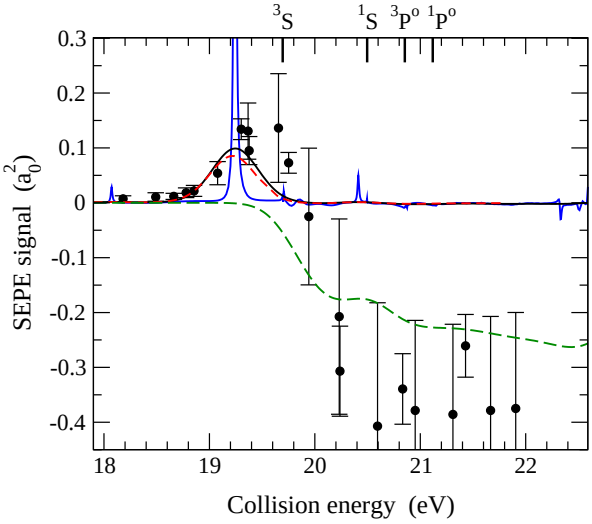

Figure 7. Comparison of theoretical and experimental SEPE signals (difference between the laser-assisted and field-free cross sections) for the production of metastable states of helium. The incident electron momentum is at 45° to the laser polarization axis. Theory: ——, SEPE signal including the contributions from excitation into the $2\,^3\widetilde{\mathrm{S}}$, $2\,^1$S and $2\,^3\widetilde{\mathrm{P}}^o$ dressed states; ——, SEPE signal, convolved with the energy spread of the incident electron beam; - - - -, convolved SEPE signal from our 5-state RMF calculation [19]; – – –, lower bound for the SEPE signal (the negative of the convolved field-free cross sections for excitation into the $2\,^3$S, $2\,^1$S and $2\,^3$P^o states). Experiment: •, [18].

Our results with and without convolution are shown in figure 7 together with those of our earlier five-state R-matrix Floquet calculation [19]. The agreement between the convolved results and the experimental values of Luan *et al* is relatively good up to the $2\,^3$S threshold, and is particularly satisfactory since the latter are on an absolute scale and no normalization procedure has had to be performed, in contrast to our previous work on SEPE in a CO_2 laser [15]. Since the SEPE signal at low energies is dominated by the $He^-(1s2s^2\,^2S)$ resonance, our present results are fairly similar to those for $\theta_{in} = 0^o$. Extending our field-free atomic basis from 5 to 11 states increases by 15 % the maximum of the SEPE signal at about 19.3 eV. It also broadens the peak towards slightly higher collision energies. The tiny structures at 19.7 eV are due to the $2\,^3$S threshold while the two small peaks at 18.1 eV and 20.4 eV are symmetrically distant by 1.17 eV from the $He^-(1s2s^2\,^2S)$ resonance. The first peak appears in the SEPE cross section with absorption of two photons, where one photon is first absorbed, leading to the temporary capture in the resonant state, followed by absorption of another photon. The second peak appears in the SEPE cross process with no net exchange of photons and corresponds to emission of one photon leading to the temporary capture in the resonant state followed by absorption of another photon. All these small structures are however completely washed out after convolution and the signal above 19.8 eV becomes negligible.

As discussed above, the peak seen below the $2\,^3$S threshold is clearly due to the $He^-(1s2s^2\,^2S)$ resonance, which in field-free scattering only appears in the elastic channel and not in any excitation channel. This implies that the various low-frequency approximations [9–12] or the semi-classical approximation [14], which attempt to relate the cross section for a particular laser-assisted excitation process to that for the same process in the absence of the laser field, will not be able to reproduce the peak. This was indeed illustrated by Luan *et al* who found that the semi-classical model of Chichkov [14] yields a SEPE signal that is positive below the $2\,^3$S threshold, but whose amplitude is about a factor four too small.

Above the $2\,^3$S threshold, the signal becomes negative, reflecting the fact that the cross section with laser *on* is smaller than that with laser *off*. Similar features are observed for SEPE in a CO_2 laser field [15] and can be explained in a simplistic way as follows: for a low-frequency laser, the SEPE cross section is related to the field-free cross section through a convolution with a cylindrical Bessel function arising from the dressing of the collisional electron by the laser field. Below threshold, the field-free cross section is zero and hence the SEPE cross section just above threshold tends to be smaller than the field-free excitation cross section. This model, applicable for a low frequency laser, is not valid for a Nd:YAG laser but a decrease in the SEPE signal above threshold would not be unexpected. The broken curve in figure 7 represents the lower possible limit of the theoretical SEPE signal: since the signal is the difference of the cross sections with the laser on and with it off, this lower limit corresponds to the hypothetical case where no metastable atoms are detected with the laser on, and is thus given by the negative of the field-free cross section for production of metastable states. It is thus surprising that the measured signal is systematically lower than this limit, even taking into account the large experimental error bars, as it would imply a negative laser-assisted cross section. This is even more obvious from figure 5 in the paper by Luan *et al* where they presented their measured field-free cross section for production of metastable atoms together with the SEPE signal over a wider range of collision energy, up to 100 eV.

Luan *et al* attributed this apparent loss of metastable signal to multiphoton ionization of the excited helium atoms produced by the SEPE process. They estimated from experimental parameters that 6% of the metastables were lost, corresponding to an effective multiphoton ionization rate of about $7 \times 10^6\,\mathrm{s}^{-1}$. The lack of theoretical data did not allow them to draw any conclusion about which, if indeed any, multiphoton ionization processes could explain their measurements. To try to assess the possible role of multiphoton ionization in their experiment, we now present a brief study of this process using the R-Matrix Floquet method.

4. Multiphoton ionization of triplet states of helium

Since many experimental parameters such as the laser intensity and atomic beam profiles are unknown to us, we perform only a simple model calculation with a frozen $He^+(1s)$ core. The energies of the five lowest triplet states of helium, obtained using the R-

Table 3. Energies in atomic units of the five lowest triplet states of helium. The theoretical values, obtained using the R-matrix Floquet method for zero laser intensity and keeping the $He^+(1s)$ core fixed, are compared with the accurate, non-relativistic energies taken from chapter 11 of [26].

	Frozen $He^+(1s)$	Accurate
1s2s 2^3S	−2.17425	−2.17523
1s2p 2^3P^o	−2.13132	−2.1323316
1s3s 3^3S	−2.06849	−2.06869
1s3p 3^3P^o	−2.05758	−2.0575808
1s3d 3^3D	−2.05557	−2.05564

matrix Floquet method for zero laser intensity, are presented in table 3. Due to the lack of correlation, especially in the ground state, the energies of the field-free states are slightly too high. The $2\,^3S$ and $2\,^3P^o$ states require respectively 5 and 4 photons of energy $\omega = 0.043$ au to ionize. The energies of these two states differ by almost one photon energy, while the $2\,^3P^o$ state is itself in near 3-photon resonance with the $He(1s12\ell)$ Rydberg states, particularly those with $\ell \neq 0$.

In figure 8, we present the real part of the quasi-energies obtained in the triplet symmetry for $\mathcal{M}_\mathcal{L} = 0$ as a function of intensity for a Nd:YAG laser field. The figure shows the only crossings involving the $2\,^3\widetilde{S}$ and $2\,^3\widetilde{P}^o$ states in the range of intensity from 10^9 to $10^{10}\,W\,cm^{-2}$. The lower crossings correspond to 4-photon resonances of $2\,^3\widetilde{S}$ with the $12\,^3D$ and $12\,^3G$ Rydberg states, while the upper crossings correspond to 3-photon resonances of $2\,^3\widetilde{P}^o$ and the same Rydberg states. The crossings with $12\,^3G$ are avoided, indicating a relatively strong interaction between the states. The interaction with $12\,^3D$ is very weak, as might be expected from the usual propensity rules for photoabsorption; the $12\,^3D$ curve is perturbed by the $2\,^3\widetilde{S}$ and $2\,^3\widetilde{P}^o$ states but not enough to give rise to an avoided crossing. We also note that the interaction with the Ryberg states of the $2\,^3\widetilde{S}$ and $2\,^3\widetilde{P}^o$ are very similar, due to their strong AC Stark mixing.

The ionization rates correspond to twice the magnitude of the imaginary part of the quasi-energies and are shown in figure 9. Away from resonance, the ionization rates of the $2\,^3\widetilde{S}$ and $2\,^3\widetilde{P}^o$ states are very small, of the order of a few 10^{-10} au. The interactions with the $1s12d\,^3D$ Rydberg state (not shown) are very weak, only giving rise to a small perturbation in the imaginary part of the associated quasi-energy. The enhancement of the total ionization rate is therefore exclusively due to the resonances with the $1s12g\,^3G$ state. In the region of these crossings, the ionization rates increase to almost 6×10^{-8} au, which corresponds to about $2\times10^9\,s^{-1}$. While this rate is much higher than that estimated by Luan *et al*, it only occurs in a very narrow range of laser intensity. It is therefore difficult to estimate how efficient the 1+3+1 and 3+1 REMPI processes would be in removing excited atoms from the atomic beam: a reliable estimation would require a detailed knowledge of the experimental conditions, in particular the laser intensity profile but also the velocity distribution of the atoms [31]. In addition, the

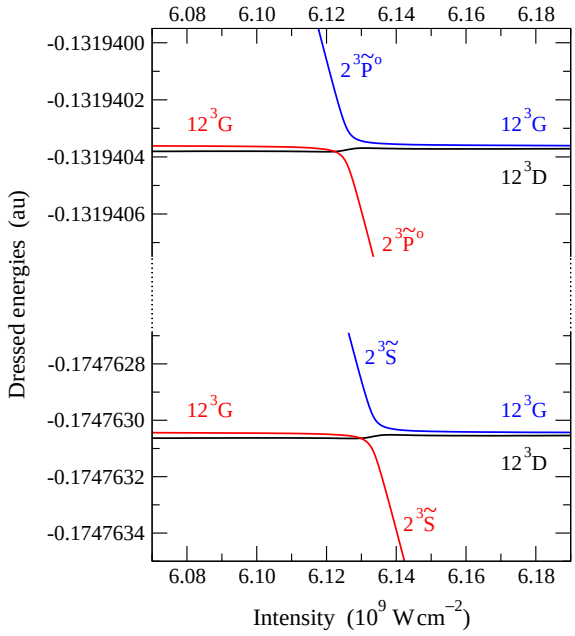

Figure 8. Dressed energies of the $2\,^3\widetilde{S}$ and $2\,^3\widetilde{P}^o(M_f{=}0)$ states of helium in a Nd:YAG laser field as a function of intensity, in the region of the four-photon (lower curves) and three-photon (upper curves) resonances with the 1s12d ^{3}D and 1s12g ^{3}G Rydberg states. No other resonances are seen in the range of intensities between 10^9 and 10^{10} W cm^{-2}.

crossings are sensitive to the intensity of the laser field: the position of the Rydberg states with respect to the ionization threshold hardly changes, while the $2\,^3\widetilde{S}$ and $2\,^3\widetilde{P}^o$ states tend to become more strongly bound as the intensity increases. The one-photon ionization rate of the $12\,^3G$ states is a fairly linear function of the laser intensity.

It should be noted that in a more accurate calculation, these quasi-energy crossings will occur at different intensities than those found here, and the REMPI process may pass via other Rydberg states than through the $n = 12$ manifold as the atom moves through the laser beam. It is however likely that REMPI processes played a important role in reducing the SEPE signal in the experiment. Their effect below the $2\,^3S$ threshold may not be so apparent because of the dominant contribution of the $He^-(1s2s^2\,^2S)$ resonance, while above threshold, it further reduces the small number of metastable atoms that reach the detector, inducing an apparent SEPE signal that is too negative.

5. Conclusion

We have extended our previous study of excitation of helium into the $1s2s\,^{3,1}S$ and $1s2p\,^3P^o$ metastable states by electron impact in the presence of a Nd:YAG laser field in order to compare with the experimental data by Luan *et al* [18]. All calculations were performed using the *R*-matrix Floquet method which is particularly well suited for investigating atomic collisions with strong electronic and radiative couplings. The

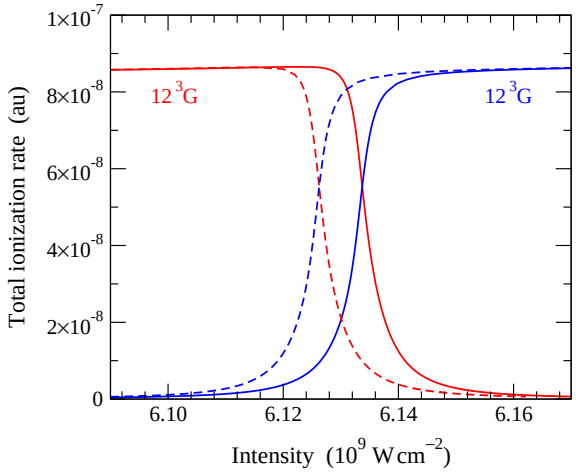

Figure 9. Total ionization rates at the resonance between the $2\,^3\widetilde{\mathrm{S}}$ (solid lines) and the $2\,^3\widetilde{\mathrm{P}}^{\mathrm{o}}(M_{\mathrm{f}}{=}0)$ (dashed lines) states of helium with the $1\mathrm{s}12\mathrm{g}\,^3\mathrm{G}$ Rydberg states.

excitation of the ground ^{1}S state to $2\,^3$S and $2\,^3\mathrm{P}^{\mathrm{o}}$ states can occur only through exchange of the collisional electron with one of the target. The atomic basis to describe the helium target was extended from 5 to 11 states to improve the convergence of our calculation above the He(1s2ℓ) thresholds. Calculations were also performed for total magnetic quantum number $\mathcal{M}_{\mathcal{L}} > 0$ in order to investigate collision geometries with electron incoming at non-zero angles with respect to the direction of laser polarization.

We have demonstrated that the $\mathrm{He}^-(1\mathrm{s}2\mathrm{s}^2\,^2\mathrm{S})$ resonance plays a leading role in the simultaneous electron-photon excitation (SEPE) process below the $2\,^3$S threshold. The photon energy of the Nd:YAG laser coincides almost exactly with the energy difference between the $2\,^3$S and $2\,^3\mathrm{P}^{\mathrm{o}}$ states, giving rise to a strong AC Stark mixing between these two states. Partial SEPE cross sections are strongly affected by this dynamical mixing but when summed over all possible final states, the difference of the total cross section with respect to the field-free excitation cross section appears mainly near the $\mathrm{He}^-(1\mathrm{s}2\mathrm{s}^2\,^2\mathrm{S})$ resonance and its satellite lines due to exchange of photons. After convolution over the energy dispersion of the incident electron beam, the theoretical SEPE signal (difference between the cross section with and without laser field) is in good agreement with the experimental data of Luan *et al* [18] below the $2\,^3$S threshold. Above this threshold, the measured SEPE signal is so negative that the cross section for production of metastable states in the presence of the laser field would appear to be negative. We have shown in a model calculation that 1+3+1 resonance-enhanced multiphoton ionization of the $2\,^3$S state via the $2\,^3\mathrm{P}^{\mathrm{o}}$ and $12\,^3$G Rydberg state can yield a very high ionization rate, albeit over a very narrow range of intensities, suggesting that this process is indeed an important mechanism for signal loss for time-of-flight spectroscopy for metastable production.

References

[1] Mason N J and Newell W R 1987 *J. Phys. B: At. Mol. Opt. Phys.* **20** L323–L326
[2] — 1989 *J. Phys. B: At. Mol. Opt. Phys.* **22** 777–96
[3] — 1990 *J. Phys. B: At. Mol. Opt. Phys.* **23** L179–L182
[4] Wallbank B, Holmes J K, LeBlanc L and Weingartshofer A 1988 *Z. Phys. D* **10** 467–472
[5] Wallbank B, Holmes J K and Weingartshofer A 1989 *J. Phys. B: At. Mol. Opt. Phys.* **22** L615–L619
[6] — 1990 *J. Phys. B: At. Mol. Opt. Phys.* **23** 2997–3005
[7] Jetzke S, Faisal F H M, Hippler R and Lutz H O 1984 *Z. Phys. A* **315** 271–276
[8] Jetzke S, Broad J and Maquet A 1987 *J. Phys. B: At. Mol. Phys.* **20** 2887–2897
[9] Mittleman M H 1980 *Phys. Rev. A* **21** 79–84
[10] Geltman S and Maquet A 1989 *J. Phys. B: At. Mol. Opt. Phys.* **22** L419–L425
[11] Maquet A and Cooper J 1990 *Phys. Rev. A* **41** 1724–1727
[12] Mittleman M H 1993 *J. Phys. B: At. Mol. Opt. Phys.* **26** 2709–2716
[13] Fainstein P D, Maquet A and Fon W C 1995 *J. Phys. B: At. Mol. Opt. Phys.* **28** 2723–2728
[14] Chichkov B N 1990 *J. Phys. B: At. Mol. Opt. Phys.* **23** L333–L338
[15] Dunseath K M and Terao-Dunseath M 2011 *J. Phys. B: At. Mol. Opt. Phys.* **44** 135203
[16] deHarak B A, Ladino L, MacAdam K B and Martin N L S 2011 *Phys. Rev. A* **83** 022706
[17] Mason N 1993 *Rep. Prog. Phys.* **56** 1275–1346
[18] Luan S, Hippler R and Lutz H O 1991 *J. Phys. B: At. Mol. Opt. Phys.* **24** 3241–3249
[19] Terao-Dunseath M, Dunseath K M, Charlo D, Hibbert A and Allan R J 2001 *J. Phys. B: At. Mol. Opt. Phys.* **34** L263–L270
[20] Burke P G, Francken P and Joachain C J 1990 *Europhys. Lett.* **13** 617–622
[21] — 1991 *J. Phys. B: At. Mol. Opt. Phys.* **24** 761–790
[22] Burke P G 2011 *R*-matrix Theory of Atomic Collisions: Application to Atomic, Molecular and Optical Processes (Springer)
[23] Joachain C J, Kylstra N J and Potvliege R M 2012 Atoms in Intense Laser Fields (Cambridge University Press)
[24] Terao-Dunseath M and Dunseath K M 2002 *J. Phys. B: At. Mol. Opt. Phys.* **35** 125–140
[25] Kroll N M and Watson K M 1973 *Phys. Rev. A* **8** 804–809
[26] Drake G W F, ed. 2006 Handbook of Atomic, Molecular and Optical Physics (Springer)
[27] Ralchenko Y, Kramida A E, Reader J and the NIST ASD Team 2010 NIST Atomic Spectra Database
[28] Nehari D, Holmes J K, Dunseath K M and Terao-Dunseath M 2010 *J. Phys. B: At. Mol. Opt. Phys.* **43** 025203
[29] Hibbert A 1975 *Comput. Phys. Commun.* **9** 141–172
[30] Dunseath K M, Terao-Dunseath M and Bourhis G 2005 *Phys. Rev. A* **72** 033410
[31] Génévriez M, Urbain X, Terao-Dunseath M and Dunseath K M 2013 11th European Conference on Atoms, Molecules and Photons (Aarhus, Denmark), poster T5-13